Resilience-oriented operation of power systems
Hierarchical partitioning-based approach

Zare Oskouei, Morteza; Mehrjerdi, Hasan; Babazadeh, Davood; Teimourzadeh Baboli, Payam; Becker, Christian; Palensky, Peter

DOI
10.1016/j.apenergy.2022.118721

Publication date
2022

Document Version
Final published version

Published in
Applied Energy

Citation (APA)
Zare Oskouei, M., Mehrjerdi, H., Babazadeh, D., Teimourzadeh Baboli, P., Becker, C., & Palensky, P. (2022). Resilience-oriented operation of power systems: Hierarchical partitioning-based approach. *Applied Energy*, *312*, 1-11. Article 118721. https://doi.org/10.1016/j.apenergy.2022.118721

Applied Energy 312 (2022) 118721

Contents lists available at ScienceDirect

Applied Energy

journal homepage: www.elsevier.com/locate/apenergy

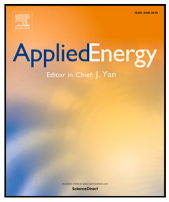

Resilience-oriented operation of power systems: Hierarchical partitioning-based approach

Morteza Zare Oskouei [a,*], Hasan Mehrjerdi [a], Davood Babazadeh [b], Payam Teimourzadeh Baboli [c], Christian Becker [b], Peter Palensky [d]

[a] Department of Electrical Engineering, Qatar University, Doha, Qatar
[b] Institute of Electric Power and Energy Technology, Hamburg University of Technology, Hamburg, Germany
[c] R&D Energy Division, OFFIS – Institute for Information Technology, Oldenburg, Germany
[d] Intelligent Electrical Power Grids, Delft University of Technology, 2600 Delft, The Netherlands

ARTICLE INFO

Keywords:
Local operation
Nested strategy
Partitioning mechanisms
Privacy-preserving
Resiliency evaluation

ABSTRACT

As an achievement of innovations resulting from partitioning mechanisms, these mechanisms can contribute to the more flexible operation of power systems in local communities. The ever-increasing frequency and severity of unexpected real-time failures have created challenges for partitioned-based power system operators, affecting each partition's resiliency. With this in mind, this paper presents an adaptive local operation strategy (ALOS) for resilient scheduling of the renewable-dominated partitioned-based power systems under normal and islanding modes in a decentralized manner. The main objective of the developed ALOS lies in reaching an affordable preparedness level in each partition to deal with unscheduled islanding mode, which can occur subsequent to real-time failures at common lines between adjacent partitions on transmission level. To this end, a set of resilience-target constraints is presented to prepare sufficient spinning reserve capacity in each partition to ensure continuity of supply during islanding mode. The proposed strategy is formulated as a two-stage stochastic mixed-integer linear program (MILP), and the nested formation algorithm is employed to execute it in a hierarchical fashion based on the privacy-preserving protocols. Besides, the tri-state compressed air energy storage (CAES) system is also included in the proposed strategy to mitigate the negative consequences caused by real-time failures and uncertain sources. Numerical results conducted on the IEEE 30-bus test system reveal that the proposed ALOS can enhance the resilience of each partition in responding to unscheduled islanding mode by efficiently utilizing all available capacities on the generation side. Furthermore, the DIgSILENT PowerFactory is used to identify the worst possible series of events and to evaluate the effectiveness of the proposed resilience-promoting proactive strategy in dealing with these events.

1. Introduction

1.1. Motivation and aim

The partitioning mechanisms can help power system planners to accelerate the implementation of decentralization and to reform power systems development plans [1]. The benefits of decomposing large-scale power systems into multiple partitions have been extensively studied from the energy efficiency and flexibility standpoints [2]. These mechanisms have implications on how the power systems are being operated. Towards this end, different partitioning mechanisms in interaction with the operational constraints have been developed with the aim of maximizing the self-sufficiency index in each partition considering high penetration of renewable energy sources (RESs), e.g., [3, 4]. Recently, the increasing rates of unexpected events have posed serious operational challenges for renewable-dominated partitioned systems [5]. For instance, the European Network of Transmission System Operators for Electricity (ENTSO-E) [6] has reported an unexpected incident that occurred on 8 January 2021 between two private partitions of ENTSO-E caused these partitions to split into two asynchronous zones. This event can confirm that there is no guarantee to detect and prevent real-time failures through the adopted defense plans in each partition before the malfunction occurs [7].

In response to the mentioned challenge, resilience enhancement strategies at the pre-disruption phase can mitigate the consequence of unexpected events in partitioned-based power systems. However, it is

* Corresponding author.
E-mail address: morteza.z@qu.edu.qa (M. Zare Oskouei).

https://doi.org/10.1016/j.apenergy.2022.118721
Received 24 October 2021; Received in revised form 18 January 2022; Accepted 7 February 2022
Available online 25 February 2022

Nomenclature

A. Indices/Set

$i, j/\mathcal{I}$	Indices/set of electric buses.
$l/\mathcal{L}$	Index/set of the existing partitions.
$t/\mathcal{T}$	Index/set of hourly time slots.
s/S	Index/set of generated scenarios in real-time decisions.
Ω_l	Set of buses that are located at partition l.

B. Superscripts

ch, dis, si	Superscripts for charging, discharging, and simple cycle modes.
d	Superscript for electrical loads.
cl, ncl	Superscripts for critical and non-critical electrical loads.
isl	Superscript for unscheduled islanding mode.
g, k	Superscripts for thermal units and tri-state CAES systems.
v, w	Superscripts for photovoltaic parks and wind farms.

C. Parameters

b, g	Susceptance and conductance of the line connecting buses i and j.
c	Number of sides of regular polygons used to linearize nonlinear AC power flow equations.
h	Number of tangent hyperplanes used to linearize cosine function via polyhedron relaxation.
MC^{exp}, MC^{co}	Maximum participation capacity of tri-state CAES systems in expanding and compressing modes.
PF	Load power factor.
$R^{\uparrow}$, $R^{\downarrow}$	Ramp-up and ramp-down limits of thermal units.
VC^{exp}, VC^{co}	Variable operation and maintenance costs for expanding and compressing modes.
$VOLL$	Value of loss load.
β	Percentage of usable capacity of common lines between adjacent partitions.
λ^{ng}	Natural gas price.
λ^{re}	Penalty price for renewable power curtailment.
ψ	Heat ratio of tri-state CAES systems.
η	Efficiency coefficient of tri-state CAES systems.
τ, $\Delta\tau$	Fault duration time and permissible adjusting time of thermal units after islanding state.
ϕ_s	Probability of scenarios.
$\underline{(\cdot)}$, $\overline{(\cdot)}$	Symbols for lower and upper limits of variables.

D. Variables

P, Q	Functions for scheduled active and reactive power in normal or islanding situations.
SE	Reservoir capacity of tri-state CAES systems.
SUC, SDC	Start-up and shut-down costs of thermal units.
V, θ	Functions for voltage magnitude and voltage angle of buses.
α	Load shedding of non-critical demands after islanding state.
ζ	Binary variable to indicate the status of thermal units and tri-state CAES systems.

not possible to increase the resilience level of partitioned systems without analyzing the behavior of each partition in a decentralized manner under variable operational conditions, i.e., normal and emergency conditions. Inspired by the issues raised, this paper aims to take a practical look at the resiliency issues in renewable-dominated partitioned-based power systems and enhance each partition's preparedness level to deal with any real-time failures on the transmission level.

1.2. Comparison to related literature

According to definitions given in the literature, resilience operation strategies have been proposed to evaluate (1) the preparedness level of power systems before any disruptive event, (2) the adequacy of systems to respond to events in an effective manner, and (3) the ability of systems to recover from such an event [8]. In general, the main motivation of the most conducted studies has been to achieve an appropriate level of technical preparedness to deal with the islanded operation effectively. Therefore, concerning the scope of this paper, the existing literature can be broadly divided into two groups.

First, some previous studies are concerned with the resilient operation of renewable integrated power systems, such as [9], a robust optimization-based decision support tool was proposed to improve the power system resilience against unexpected disasters considering variable RESs. Authors in [10] developed a two-stage decision-making framework for resilient scheduling of power systems considering the pre-contingency condition. In the same work, the energy conversion facilities were deployed to establish a stable connection between electricity and gas networks to deal with sequences of contingencies. Authors in [11] presented the resilience-oriented stochastic scheduling approach for integrated heat and power systems to increase the power system resiliency in northern Germany. In that work, the positive effects of RESs and energy conversion facilities were considered for the continuous supply of critical loads under the risk of both disruption scenarios and uncertainties. The work reported in [12] used the proactive mechanism to develop an optimal resilient scheduling scheme for radial and mesh networks. To improve the computational efficiency for resilience analysis and enhancement, studies such as [13] presented a parallel solution approach for strategic power infrastructure defense systems to withstand real-time failures. Furthermore, an outage management scheme was introduced in [14] to enhance the resilience of power systems when high-impact low-probability events occurred at the point of common coupling (PCC).

Second, some studies applied different resilience-based optimization problems for the multi-area power systems to adopt efficient defense plans against disruption events. For example, a real-time control framework was presented in [15] to support the interconnected systems power balance considering high penetration of wind power. Likewise, the impacts of establishing a global day-ahead energy management system for the multi-area power system were evaluated in [16] to satisfy resiliency requirements during unscheduled islanding operation. In that work, a centralized control mechanism was employed to reach the resilience performance of each area under hybrid attacks at common boundaries. Other studies, e.g., in [17,18], presenting optimal

resilient scheduling strategies to guarantee the resilient operation of interconnected bulk systems and/or medium-voltage systems against real-time failures considering uncertainties of RESs and loads. Additionally, the mentioned studies were implemented through a day-ahead centralized operation problem that tried to minimize the total operation cost in both normal and emergency periods. On the other hand, authors in [19] took another strategy and developed a layered control system for resilient management of a set of interconnected systems to restrict load shedding amounts and decrease the amount of renewable power curtailment during the emergency period. In another effort, authors in [20] presented a privacy-preserving strategy for day-ahead optimal scheduling of the resilient multi-area power system considering feasible islanding operation mode.

There are several important shortcomings (**SHs**) in the aforementioned literature that necessitate further studies. (**SH1**) The surveyed studies in the first group, i.e., [9–14], did not mention how the presented strategies can be extended for each partition of large-scale systems in a decentralized manner. In contrast, herein, our focus is on the resilient operation of interconnected partitions to mitigate each partition's risk of islanded operation separately. (**SH2**) The presented studies in [15–18] were limited to centralized optimization approaches to adopt an optimal resilient scheduling scheme for multi-area interconnected power systems. Such approaches are more completely at odds with privacy-preserving issues at the highest decision-making levels, which consist of independent transmission companies (TRANSCOs). (**SH3**) None of the studies reviewed considered the congestion effects on the common lines between interconnected power systems in the presented resilient scheduling schemes. Under these circumstances, the interdependence between different interconnected areas in developing preventive actions to deal with disruption events will be ignored, which may lead to infeasible results that are not realizable in practical systems. (**SH4**) The aforementioned studies did not mention that how distributed control algorithms and partitioning concepts can be integrated into resilience-promoting programs designed for renewable-dominated power systems. (**SH5**) A majority of the literature failed to evaluate the synergic effects of fast-ramping backup resources, such as tri-state compressed air energy storage (CAES), in the resilient operation of the partitioned-based power systems on the transmission level.

1.3. Technical contributions and paper structure

To tackle the aforementioned research gaps, we are interested in answering a series of questions related to the resilient operation of partitioned-based power systems: (1) How can preventive measures be individually implemented for interconnected partitions to deal with unexpected events that may occur at any real-time scheduling interval? (2) How to ensure that the used preventive measures are properly enforced in resilience-oriented strategies while not increasing the problem's computational burden? (3) How can a decentralized resilient scheduling scheme adopted for a partition affect the optimal operation of resources on other partitions? (4) How can the promoted energy conversion facilities effectively meet the resiliency requirements in each partition?

Therefore, to the best of our knowledge, it is fair to say that there is no prior study for the resilient operation of renewable-dominated power systems by relying on the partitioning mechanism and distributed control architecture on the transmission level. The presented method in this study is fundamentally different from the prior work, e.g., due to the need to address the survivability performance of each partition in the face of unscheduled islanding mode, which can occur subsequent to real-time failures. Moreover, the presented formulations in this study introduce several new challenges on employing preventive measures in a decentralized manner for interconnected partitions by relying on the privacy-preserving issues, real-time session applications, and multi-carrier energy conversion facilities, that are not previously addressed simultaneously. Accordingly, the major contributions and attributes of this paper can be expressed as follows:

1. *Adaptive Local Operation Strategy (ALOS) Design:* We propose an ALOS for the real-time scheduling of each formed partition in the large-scale power systems under normal and islanding situations considering the high penetration level of RESs. The proposed ALOS is executed by applying the nested formation algorithm and considering operational and technical constraints in each partition in a decentralized manner. Furthermore, the uncertainties arising from the RESs and demands are realized through the two-stage stochastic approach in real-time sessions.
2. *Local Resilience-based Scheme:* We adopt local preventive measures in the context of the proposed ALOS to increase the resilience of each partition to deal with real-time failures that may be occurring at strategic points, i.e., common lines between adjacent partitions, as well as to withstand uncertain fluctuations. The preventive measures are embedded by providing a sufficient capacity of spinning reserve obtained from local resources in each partition to survive all critical loads and achieve the optimal shedding rate of non-critical loads under unscheduled islanding mode. For this purpose, the role of tri-state CAES, as the resilience resource, in timely and effective response to real-time failures is investigated. All these measures are in line with the goals set by power system operators to preserve the privacy of the multi-area interconnected power systems in a hierarchical fashion.
3. *Insightful Analyzes:* Comprehensive and insightful case studies are presented to analyze the impact of the proposed ALOS on the resilient operation of the partitioned-based power system. For example, we demonstrate that how the maximum transmission power limit between adjacent partitions can affect the local scheduling policies of each partition and prevent technically infeasible solutions in an uncertain environment. From the standpoint of computational efficiency, since the adopted strategy satisfies the resiliency requirements locally, so the problem's computational burden in real power grids consisting of several partitions will be acceptable. Moreover, unlike previous studies, the contingency analysis is implemented by means of the unique features of the DIgSILENT PowerFactory to evaluate the accuracy and feasibility of the proposed strategy against a series of intense events.

The rest of this paper is organized as follows. Section 2 first provides preliminaries on the ALOS and then lists the assumptions made to implement this strategy. Next, the mathematical formulas for accurate modeling of the proposed ALOS are presented in Section 3. Section 4 presents the case studies and simulation results, and finally, the conclusions of this study are outlined in Section 5.

2. Framework description

Let us consider a power system consisting of the set $I = \{1, 2, \ldots, \mathcal{L}\}$ of $\mathcal{L}$ interconnected partitions, such as the one in Fig. 1. Each partition ($\forall I$) possesses thermal units, wind farms (WFs), photovoltaic (PV) parks, tri-state CAES systems, as well as critical and non-critical loads. According to some strong evidence, each partition may experience unscheduled islanding mode, which could be triggered by real-time failures such as cyber–physical attacks at common lines between adjacent partitions, cascaded tripping of common lines, etc. Therefore, it is necessary to enhance the resilience of each partition by taking preventive measures before islanding occurrence in real-time sessions. One of the effective preventive measures is to increase the preparedness of each partition by preparing a sufficient capacity of spinning reserve in different locations. Based on the proposed ALOS, each partition seeks to provide spinning reserve (i.e., obtained from local thermal and tri-state CAES units) equivalent to the exchanged power (received or delivered) with an adjacent partition(s). In addition, the use of tri-state CAES units enables each partition to take advantage of existing

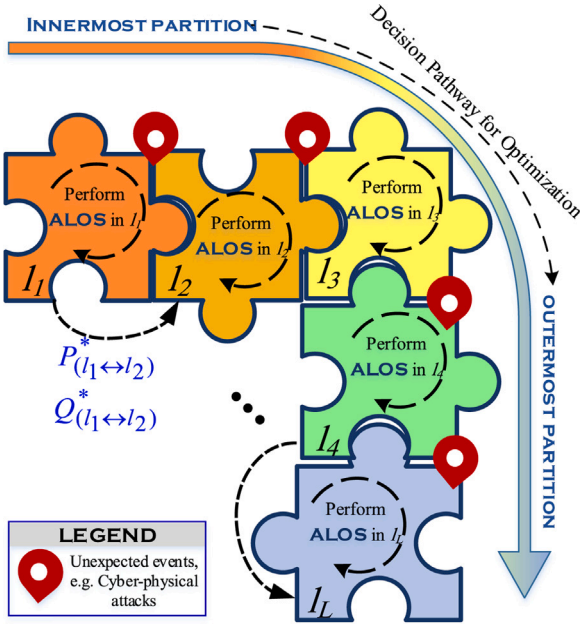

Fig. 1. Schematic illustration of the proposed ALOS in a partitioned system with l partitions.

opportunities in gas networks in simple-cycle mode to mitigate the negative consequences caused by real-time failures. By solving the proposed ALOS, the outcomes not only guarantee the resilience of each partition but also mitigates the intermittent nature of RESs and demands.

The proposed ALOS is executed using the nested formation algorithm in a decentralized manner. The nested formation algorithm has been used for different purposes in several studies, further details on this algorithm can be found in [20]. This algorithm must be executed from the innermost to the outermost partitions according to the order assigned to each partition. It should be noted that at the partitioned transmission networks, the use of nested formation algorithm means the implementation of the optimization problem in a hierarchical manner from the most critical partition (i.e., innermost partition) to the non-critical partition (i.e., outermost partition). Therefore, it is not necessary for one partition to be placed inside another partition. As shown in Fig. 1, firstly, partition $l1$ must execute the ALOS in the form of the nested formation algorithm, and then inform the adjacent partition(s), i.e., $l2$, about the amount of exchanged active and reactive power (surplus/deficit). The surplus (deficit) active and reactive power existing in the inner level partition, e.g., $l1$, is reflected as a resource (load) to the outer level partition(s), e.g., $l2$, at each time t. In this regard, to execute this strategy in lth partition, operation data of other partitions are not required. Hence, the proposed ALOS provides a proper platform to meet the privacy-preserving challenges under the collaborative operation of adjacent partitions.

2.1. Assumptions

The list of assumptions made in this paper for mathematical modeling of the proposed ALOS is as follows.

1. A prerequisite for implementing the ALOS is decomposing the large-scale power systems into several optimal partitions. For this purpose, the efficient algorithm presented in [4] is used to partition the renewable-dominated power system and the obtained results are considered as input data for the ALOS. Details of the partitioning mechanism can be found in [4].
2. The proposed ALOS aims to ensure the resilience of each partition under the worst-case realization of incidents. Therefore, it is assumed that each partition must be switched to the islanding operation mode during the emergency condition. As an example, in Fig. 1, partition $l3$ can exchange power with adjacent partitions, i.e., $l2$ and $l4$, in normal operation mode. According to this example, we assume that $l3$ will be disconnected from partitions $l2$ and $l4$ during an emergency condition at the same time. In reality, the probability of this scenario is very low, but with this assumption, the proposed ALOS will be robust to other emergency conditions, especially when a partition becomes two new partitions.
3. To implement the nested algorithm, various indicators, e.g., the size of each partition or the number of critical loads located in each partition, can be used to sort existing partitions, from the innermost to the outermost partitions. Herein, it is assumed that the innermost partition has the smallest size and vice versa, the outermost partition has the largest size. The sequence of operation can affect the simulation results in normal operation mode. But since it is assumed that in the emergency situation all partitions are operated in islanding mode, therefore, the sequence of operation will have no effect on the emergency mode results.

2.2. Scheduling horizons

In this paper, the developed ALOS must simultaneously address two operation modes, i.e., normal and emergency (unscheduled islanding) operation modes. The normal operation scheduling horizon $t = \{1, 2, \ldots, \mathcal{T}\}$ is taken as a real-time scheduling problem, and divided into $\mathcal{T}$ time slots. On the other hand, the emergency operation scheduling horizon is specified by τ, which covers a short time period, e.g., 10 min. According to the developed ALOS, the emergency period can occur at any real-time scheduling interval, i.e., $\tau \subset \mathcal{T}$, and does not include a specific time slot.

3. Problem formulation

The mixed-integer linear programming (MILP) formulation of the developed ALOS is provided in the following sub-sections for the partitioned-based power systems.

3.1. Objective function

As stated, the proposed ALOS must be sequentially run on each partition to optimize the local resources as well as to determine the optimal power trade schedule of each partition with the adjacent partitions in a decentralized manner. In this regard, all partitions seek common objectives, namely to minimize total operation cost in both normal and islanding conditions, minimize load shedding rate of non-critical loads in the islanding operation, and survive all critical loads, considering privacy provisions. Therefore, the proposed two-stage resilience-oriented stochastic model that describes the cost-efficient operation of each

partition l is as follows.

$$
\begin{aligned}
Min:{}_{\mathrm{DV}}\, TC_l = {} & \sum_{t\in\mathcal{T}}\sum_{i\in\Omega_l}\Bigg[\Bigg(\underbrace{SUC_i^g[t]+SDC_i^g[t]}_{(1a)}\Bigg) \\
& + \sum_{s\in S}\phi_s\cdot\Bigg(\underbrace{F^g(P_{i,s}^g[t])}_{(1b)}+\underbrace{\lambda^{ng}(P_{i,s}^{k,dis}[t]\cdot\psi^{k,dis}+P_{i,s}^{k,si}[t]\cdot\psi^{k,si})}_{(1c)} \\
& \underbrace{+VC^{\exp}(P_{i,s}^{k,dis}[t]+P_{i,s}^{k,si}[t])+VC^{co}(P_{i,s}^{k,ch}[t]+P_{i,s}^{k,si}[t])}_{(1d)} \\
& + \underbrace{\lambda^{re}(\tilde{P}_{i,s}^{w}[t]+\tilde{P}_{i,s}^{v}[t])}_{(1e)}+\underbrace{(VOLL\cdot\alpha_{i,s}^{d,ncl}[t]\cdot P_{i,s}^{d,ncl}[t])}_{(1f)}\Bigg)\Bigg], \forall l
\end{aligned}
\tag{1}
$$

In line with the first stage decisions, (1a) is related to the costs of start-up and shut-down of thermal units. The first stage is independent of the stochastic program and optimizes the thermal unit schedules. The second stage of the objective function consists of five terms that consider the uncertainties in power generation from RESs and loads. (1b) stands for the cost that originates from the operation of thermal units. (1c) and (1d) denote the operational and maintenance costs of tri-state CAES systems. $P_{i,s}^{k,si}[t]$ in (1c) and (1d) represents the generated power in the simple-cycle mode, under which the tri-state CAES system runs as a gas turbine. The wind and solar curtailment penalties are given by (1e). Finally, (1f) is related to the non-critical load shedding cost under islanding conditions. To maximize the resilience level of each partition, its lost non-critical load should be minimized. In (1e) and (1f), λ^{re} and $VOLL$ must be considered large enough to avoid any curtailment in normal and islanding conditions. Since the main objective of the proposed ALOS is to serve as much non-critical load as possible during unscheduled islanding mode, the amount of curtailed renewable power in this mode must reach zero. Therefore, only the non-critical load shedding cost is considered in emergency operation mode. Moreover, because all existing partitions belong to the same power system, the cost of power exchange between adjacent partitions is neglected in the ALOS. The decision variable set of the model is $DV = \left\{ \zeta_i^g[t], P_{i,s}^g[t], P_{i,s}^{k,dis}[t], P_{i,s}^{k,si}[t], P_{i,s}^{k,ch}[t], \tilde{P}_{i,s}^{w}[t], \tilde{P}_{i,s}^{v}[t], \alpha_{i,s}^{d,ncl}[t] \right\}$.

Note that the cost function defined in (1) is indexed by l, meaning that it must be held separately for each partition under different equality and inequality operational limitations. These limitations are expressed in the following sub-sections.

3.2. Thermal units operation constraints

All of the operational constraints related to the thermal units, including the minimum and maximum generation, minimum up and downtimes limits, and ramp rates of each unit in continuous time periods, are considered in the ALOS, which can be found in [21].

3.3. CAES operation constraints

The operation of tri-state CAES systems is defined by (2a)–(2d). The simple-cycle, discharging and charging rates of tri-state CAES systems are limited as presented in (2a). It should be noted that $P_{i,s}^{k,si}[t]$, $P_{i,s}^{k,dis}[t]$, and $P_{i,s}^{k,ch}[t]$ are the positive variables. Binary variables $\zeta_{i,s}^{k,si}[t]$, $\zeta_{i,s}^{k,dis}[t]$, and $\zeta_{i,s}^{k,ch}[t]$ guarantee that CAES systems operate in only one operating mode for any scheduling period, as provided in (2b). The energy stored in tri-state CAES systems during time slot t can be calculated by (2c). The set of constraints (2d) imply that the amount of energy stored in tri-state CAES systems at each time slot should be within the permitted range. Also, the energy that is stored in each tri-state CAES system at the end of the scheduling period, i.e., $\mathcal{T}$, must be equal to the initial state of charge of the same system.

$$
\begin{bmatrix} P_{i,s}^{k,si}[t] \\ P_{i,s}^{k,dis}[t] \\ P_{i,s}^{k,ch}[t] \end{bmatrix} \le \begin{bmatrix} MC_i^{k,\exp}\cdot\zeta_{i,s}^{k,si}[t] \\ MC_i^{k,\exp}\cdot\zeta_{i,s}^{k,dis}[t] \\ MC_i^{k,co}\cdot\zeta_{i,s}^{k,ch}[t] \end{bmatrix}, \forall t,s,i\in\Omega_l, \tag{2a}
$$

$$
\zeta_{i,s}^{k,si}[t]+\zeta_{i,s}^{k,dis}[t]+\zeta_{i,s}^{k,ch}[t]\le 1, \quad \forall t,s,i\in\Omega_l, \tag{2b}
$$

$$
SE_{i,s}^{k}[t] = SE_{i,s}^{k}[t-1]+\eta_i^{k,ch}P_{i,s}^{k,ch}[t]-\frac{P_{i,s}^{k,dis}[t]}{\eta_i^{k,dis}}, \forall t,s,i, \tag{2c}
$$

$$
\begin{cases} \underline{SE_i^k} \le SE_{i,s}^k[t] \le \overline{SE_i^k}, & \forall t,s,i\in\Omega_l. \\ SE_{i,s}^{k,ini} = SE_{i,s}^k[\mathcal{T}], & \forall s,i\in\Omega_l. \end{cases} \tag{2d}
$$

3.4. Normal operation mode constraints in real-time session

The local operational constraints for each partition l, each scenario s, and time interval t in the normal situation are described by (3a)–(3c). Constraints (3a) and (3b) represent the active and reactive supply–demand power balance at node i, respectively. In these equations, for each line (i,j) that connects the internal buses of partition l, let $P_{ij,s}[t]$ and $Q_{ij,s}[t]$ represent the local line active and reactive power flow under normal operation mode, respectively. Moreover, (i,j') refers to the cut set lines that connect partition l to adjacent partition(s) l'. So, $P_{ij',s}[t]$ and $Q_{ij',s}[t]$ denote the power flow on common lines between partitions l and l'. Assume that the *first loop* of the nested formation algorithm is assigned to partition l and the *next loop* assigned to partition l'. In these circumstances, when the ALOS is applied to partition l, $P_{ij',s}[t]$ and $Q_{ij',s}[t]$ terms play a variable role. However, when the ALOS is applied to adjacent partition(s) l', the mentioned terms are in the role of parameters, and their values must be fixed in the obtained amounts from the partition l. In addition, constraint (3c) retains the curtailment rate of each WF and PV park within the forecast values in each scenario.

$$
\begin{aligned}
& P_{i,s}^g[t]+P_{i,s}^{k,dis}[t]+P_{i,s}^{k,si}[t]-P_{i,s}^{k,ch}[t]+(P_{i,s}^{w}[t]-\tilde{P}_{i,s}^{w}[t]) \\
& \quad +(P_{i,s}^{v}[t]-\tilde{P}_{i,s}^{v}[t])-P_{i,s}^{d,cl}[t]-P_{i,s}^{d,ncl}[t] \\
& \quad = \sum_{j\in\Omega_l}P_{ij,s}[t]+\sum_{\substack{(i,j')\in \\ (l\leftrightarrow l')}}P_{ij',s}[t], \quad \forall t,s,i\in\Omega_l,
\end{aligned}
\tag{3a}
$$

$$
\begin{aligned}
& Q_{i,s}^g[t]-(PF_i^{d,cl}[t]\cdot P_{i,s}^{d,cl}[t]+PF_i^{d,ncl}[t]\cdot P_{i,s}^{d,ncl}[t]) \\
& \quad = \sum_{j\in\Omega_l}Q_{ij,s}[t]+\sum_{\substack{(i,j')\in \\ (l\leftrightarrow l')}}Q_{ij',s}[t], \forall t,s,i\in\Omega_l,
\end{aligned}
\tag{3b}
$$

$$
0\le\tilde{P}_{i,s}^{\{\cdot\}}[t]\le P_{i,s}^{\{\cdot\}}[t], \quad \forall t,s,i\in\Omega_l, \{\cdot\}=\{w,v\}. \tag{3c}
$$

3.4.1. Linearized AC power flow constraints

The power flow inside each partition in the normal condition is computed using the AC power flow model. The generalized modeling of AC power flow for line (i,j) can be expressed by (4a) and (4b).

$$
\begin{aligned}
P_{ij,s}[t] = {} & g_{ij}\cdot V_{i,s}^2[t]-V_{i,s}[t]V_{j,s}[t]\left(g_{ij}\cdot\cos(\theta_{ij,s}[t])\right. \\
& \left.+b_{ij}\cdot\sin(\theta_{ij,s}[t])\right), \forall t,s,(i,j)\in\Omega_l,
\end{aligned}
\tag{4a}
$$

$$
\begin{aligned}
Q_{ij,s}[t] = {} & -b_{ij}\cdot V_{i,s}^2[t]-V_{i,s}[t]V_{j,s}[t]\left(g_{ij}\cdot\sin(\theta_{ij,s}[t])\right. \\
& \left.-b_{ij}\cdot\cos(\theta_{ij,s}[t])\right), \forall t,s,(i,j)\in\Omega_l,
\end{aligned}
\tag{4b}
$$

Here, $\theta_{ij,s}[t]=\theta_{i,s}[t]-\theta_{j,s}[t]$. To decrease the computational burden and reach the convex formulation, the non-linear features of AC power flow are converted into a tractable MILP problem. In this regard,

non-linearities of (4a) and (4b) are tackled using first-order Taylor expansion and polyhedral programming relaxation [22]. Constraints (4c) and (4d) represent the piecewise linearized AC power flow model.

$$P_{ij,s}[t] \approx g_{ij}(V_{i,s}[t] - V_{j,s}[t] - \widetilde{\cos}(\theta_{ij,s}[t]) + 1) - b_{ij}\theta_{ij,s}[t], \forall t, s, (i,j) \in \Omega_l, \tag{4c}$$

$$Q_{ij,s}[t] \approx -b_{ij}(V_{i,s}[t] - V_{j,s}[t] - \widetilde{\cos}(\theta_{ij,s}[t]) + 1) - g_{ij} \cdot \theta_{ij,s}[t], \forall t, s, (i,j) \in \Omega_l, \tag{4d}$$

Let $\widetilde{\cos}(\theta_{ij,s}[t]) \in (\cos(\bar{\theta}_{\Delta}), 1)$ is polyhedral relaxation of $\cos(\theta_{ij,s}[t])$, which is defined by (4e) and (4f).

$$\begin{cases} \widetilde{\cos}(\theta_{ij,s}[t]) \le \left(\begin{array}{l} -\sin(u\gamma - \bar{\theta}_{\Delta})(\theta_{ij,s}[t] - u\gamma + \bar{\theta}_{\Delta}) + \\ \cos(u\gamma - \bar{\theta}_{\Delta}) \end{array} \right), \\ \widetilde{\cos}(\theta_{ij,s}[t]) \ge \cos(\bar{\theta}_{\Delta}), \\ \forall u \in \{1, 2, \dots, h\}, t, s, (i,j) \in \mathcal{I}, \end{cases} \tag{4e}$$

$$\gamma = \frac{2\bar{\theta}_{\Delta}}{(h+1)}; \qquad \bar{\theta}_{\Delta} \in (0, \pi/2) \tag{4f}$$

Here, $\bar{\theta}_{\Delta} \in (0, \pi/2)$ denotes the considered bound on the phase angle difference. The bus voltage limit and line thermal constraints are captured in (4g) and (4h).

$$\underline{V}_i \le V_{i,s}[t] \le \overline{V}_i, \quad \forall t, s, i \in \Omega_l, \tag{4g}$$

$$P^2_{ij,s}[t] + Q^2_{ij,s}[t] \le \left|\overline{S}_{ij,s}\right|^2, \quad \forall t, s, (i,j) \in \Omega_l. \tag{4h}$$

The non-linear form of (4h) is linearized using the polygonal linearization method, which is represented by (5a)–(5c) [23].

$$\left[\sin\left(\frac{2\pi n}{c}\right) - \sin\left(\frac{2\pi(n-1)}{c}\right)\right] P_{ij,s}[t] - \left[\cos\left(\frac{2\pi n}{c}\right) - \cos\left(\frac{2\pi(n-1)}{c}\right)\right] Q_{ij,s}[t] - \left|\overline{S}_{ij}\right| \sin\left(\frac{2\pi}{c}\right) \le 0, \quad \forall n \in \{1, 2, \dots, c\}, t, s, (i,j) \in \Omega_l, \tag{5a}$$

$$-\left|\overline{S}_{ij}\right| \le P_{ij,s}[t] \le \left|\overline{S}_{ij}\right|, \quad \forall t, s, (i,j) \in \Omega_l, \tag{5b}$$

$$-\left|\overline{S}_{ij}\right| \le Q_{ij,s}[t] \le \left|\overline{S}_{ij}\right|, \quad \forall t, s, (i,j) \in \Omega_l. \tag{5c}$$

3.4.2. AC power flow between partitions

The linearized AC power flow model, i.e., (4c) and (4d), must also be considered for each common line between partition l and adjacent partition(s) l'. As shown in Fig. 2, from the perspective of partition l, the adjacent partition(s) l' is considered as an external grid, i.e., $V_{j',s}[t] = 1$ and $\theta_{j',s}[t] = 0$. Therefore, (4c) and (4d) should be modified based on these values to calculate $P_{ij',s}[t]$ and $Q_{ij',s}[t]$. Given this hypothesis, when implementing the ALOS in adjacent partition(s) l', some grid code requirements at the PCC may be violated and new technical challenges may arise for adjacent partition(s). To prevent such challenges, the amount of power flow between adjacent partitions $(l \leftrightarrow l')$ should be bounded by a control coefficient, i.e., $0 < \beta \le 1$, as given in (6). With increasing the amount of β, partition l will have more degree of freedom for decision making, which may prevent some technical constraints in adjacent partition(s) l' from being satisfied.

$$P^2_{ij',s}[t] + Q^2_{ij',s}[t] \le \left|\beta \cdot \overline{S}_{ij'}\right|^2, \quad \forall t, s, (i,j') \in (l \leftrightarrow l'). \tag{6}$$

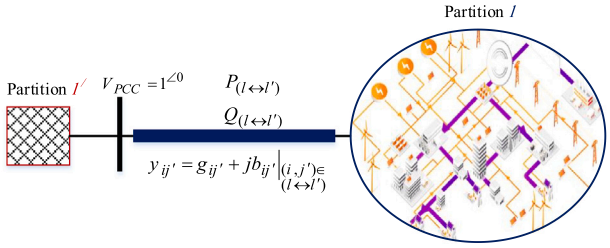

Fig. 2. Simplified representation of l' partition as seen from partition l side.

3.5. Islanding mode constraints in real-time session

Following the real-time failures at common lines between adjacent partitions, e.g., l and l', each partition must operate in the islanding mode of operation using the developed ALOS. To this end, the following resilience-target constraints must be met at any time to reach the desired level of preparedness in each partition during unscheduled islanding. Although these constraints must be locally satisfied, their effects will be indirectly reflected in the amount of exchanged power between adjacent partitions. Constraints (7a) and (7b) express the supply–demand power balance at each bus of partition l during the unscheduled islanding operation mode. It can be observed from these constraints that all terms are similar to their normal operation mode counterpart constraints, except for the amount of non-critical loads and exchanged power between adjacent partitions. The load shedding amount of non-critical loads is determined by $\alpha^{d,ncl}_{i,s}[t]$, which the upper and lower bounds of this variable are enforced by (7c). Note that constraints (4c), (4d), and (4h) must also be satisfied for the active and reactive power flow during the islanding mode, i.e., $P^{isl}_{ij,s}[t]$ and $Q^{isl}_{ij,s}[t]$. In reality, the power system can go beyond normal operation limits during islanding mode. In this regard, the bus voltage limit can be as much as ΔV^{isl}_i, about 0.05 p.u., different from the normal mode, which is expressed by (7d).

The commitment state of thermal units cannot be immediately changed in islanding mode, so these units are forced to remain in the same normal operation mode when a failure occurs. However, it is necessary that the output power of thermal units in islanding mode, i.e., $P^{g,isl}_{i,s}[t]$, be quickly adjusted based on their maximum up/down ramping rate to mitigate the power mismatch. The allowable time to adjust the output power of thermal units, i.e., $\Delta\tau$, can be determined according to the degree of importance of each partition. The set of constraints (7e) take care of these issues. $\Delta\tau$ can be changed depending on the dynamic structure of different thermal units. In addition, (7f) and (7g) represent the allowable generation capacity of thermal units in islanding mode.

Unlike thermal units, tri-state CAES systems can be switched from charging to generating status, i.e., discharging and simple-cycle modes, and vice versa immediately after an incident. The set of constraints (7h) limit the power stored/released in/from tri-state CAES systems in islanding mode. Constraint (7i) demonstrates that each CAES system must maintain the reservoir level within the allowable range until failures are cleared. According to (7i), the power output/input of each CAES system is directly related to the fault duration time, i.e., τ. In other words, τ is the predicted time by the system operator to clear the fault and recover the normal operation.

The supply rate of non-critical loads is one of the ideal indices to evaluate the resilience level under emergency conditions. In this paper, the resiliency index for each partition (RI_l) is calculated by (7j). The closer the value of RI_l to one, the stronger the resilience level of each partition.

$$P_{i,s}^{g,isl}[t] + P_{i,s}^{k,isl}[t] + P_{i,s}^{w}[t] + P_{i,s}^{v}[t] - P_{i,s}^{d,cl}[t] - (1 - \alpha_{i,s}^{d,ncl}[t])P_{i,s}^{d,ncl}[t] = \sum_{j \in \Omega_l} P_{ij,s}^{isl}[t], \quad \forall t, s, i \in \Omega_l, \tag{7a}$$

$$Q_{i,s}^{g,isl}[t] - (PF_i^{d,ncl}[t](1 - \alpha_{i,s}^{d,ncl}[t])P_{i,s}^{d,ncl}[t]) - (PF_i^{d,cl}[t] \cdot P_{i,s}^{d,cl}[t]) = \sum_{j \in \Omega_l} Q_{ij,s}^{isl}[t], \forall t, s, i \in \Omega_l, \tag{7b}$$

$$0 \le \alpha_{i,s}^{d,ncl}[t] \le 1, \quad \forall t, s, i \in \Omega_l, \tag{7c}$$

$$\underline{V_i} - \Delta V_i^{isl} \le V_{i,s}^{isl}[t] \le \overline{V_i} + \Delta V_i^{isl}, \quad \forall t, s, i \in \Omega_l, \tag{7d}$$

$$\begin{cases} P_{i,s}^{g,isl}[t] \ge P_{i,s}^{g}[t] - (\zeta_i^g[t] \cdot R_i^{g\downarrow} \cdot \Delta\tau), & \forall t, s, i \in \Omega_l, \\ P_{i,s}^{g,isl}[t] \le P_{i,s}^{g}[t] + (\zeta_i^g[t] \cdot R_i^{g\uparrow} \cdot \Delta\tau), & \forall t, s, i \in \Omega_l, \end{cases} \tag{7e}$$

$$\underline{P_i^g} \cdot \zeta_i^g[t] \le P_{i,s}^{g,isl}[t] \le \overline{P_i^g} \cdot \zeta_i^g[t], \quad \forall t, s, i \in \Omega_l, \tag{7f}$$

$$\begin{cases} Q_{i,s}^{g,isl}[t] \ge -Q_{i,s}^{g}[t] + \underline{Q_i^g} \cdot \zeta_i^g[t], & \forall t, s, i \in \Omega_l, \\ Q_{i,s}^{g,isl}[t] \le \overline{Q_i^g} \cdot \zeta_i^g[t] - Q_{i,s}^{g}[t], & \forall t, s, i \in \Omega_l, \end{cases} \tag{7g}$$

$$\begin{cases} P_{i,s}^{k,isl}[t] \le MC_i^{k,\exp} - \left(P_{i,s}^{k,si}[t] + P_{i,s}^{k,dis}[t]\right), \\ P_{i,s}^{k,isl}[t] \ge P_{i,s}^{k,ch}[t] - MC_i^{k,co}, \forall t, s, i \in \Omega_l, \end{cases} \tag{7h}$$

$$P_{i,s}^{k,isl}[t] \le \left(\frac{SE_{i,s}^{k}[t] - \underline{SE_i^k}}{\tau}\right)\eta_i^{k,dis}, \quad \forall t, s, i \in \Omega_l, \tag{7i}$$

$$RI_{l,s} = 1 - \sum_{t \in \mathcal{T}} \sum_{i \in \Omega_l} \alpha_{i,s}^{d,ncl}[t], \quad \forall l, s. \tag{7j}$$

3.6. Solution algorithm

The required input information and the solution procedure for applying the developed ALOS in partition l using the nested formation algorithm are described in detail in pseudocode 1.

Algorithm 1 Pseudo-code of the developed ALOS

Inputs:
Determine the boundaries of each partition using the presented algorithm in [4];
Specify the physical structure of each partition and technical specifications of different equipment;
$P_{i,s}^{d,cl}[t]$, $P_{i,s}^{d,ncl}[t]$, $PF_{i,s}^{d,cl}[t]$, $PF_{i,s}^{d,ncl}[t]$, $P_{i,s}^{w}[t]$, $P_{i,s}^{v}[t]$, λ^{ng}, λ^{re}, $VOLL$; $i \in \Omega_l$, $t \in \mathcal{T}$, $s \in \mathcal{S}$.
Result:
Optimal scheduling of available units in each partition;
TC_l^*, $RI_{l,s}^*$, $P_{ij',s}^*[t]$, $Q_{ij',s}^*[t]$, $P_{ij,s}^*[t]$, $Q_{ij,s}^*[t]$, $V_{i,s}^*[t]$.
Algorithm:
for l^{th} partition and $t \in \mathcal{T}$, $s \in \mathcal{S}$ **do**
Step 1) Generate different scenarios to realize the behavior of RESs and consumers in real-time decisions;
Step 2) Set $V_{j',s}[t]$ and $\theta_{j',s}[t]$ at the PCC between partitions l and l' to 1 and 0, respectively;
Step 3) Minimize TC_l, i.e., (1), s.t. (2a)–(7i);
Step 4) Enhance the resiliency index in l^{th} partition during islanding mode in real-time decisions by using (7a)–(7i).
if ALOS in l^{th} partition is feasible **then**
Go to the $(l-1)^{th}$ partition;
repeat Steps 1–4 for the ALOS in $(l-1)^{th}$ partition;
given that $P_{(l \leftrightarrow l-1)}^*$ & $Q_{(l \leftrightarrow l-1)}^*$ must be defined as input parameters for ALOS in $(l-1)^{th}$ partition;
else
ALOS in l^{th} partition is infeasible!
repeat this process **until** $l = 1$.

4. Case studies

In this section, the proposed ALOS was implemented on the IEEE 30-bus test system. The obtained simulation results were summarized and discussed in sub- Section 4.2, in which the scheduling horizon for the normal operation mode was considered 24 h with one-hour granularity.

4.1. Simulation setup

The test system has been divided into three optimal partitions, i.e., $\mathcal{L} = 3$, using the presented mechanism in [4]. The topology of each partition is shown in Fig. 3. According to the third assumption of the ALOS (see 2.1), the first loop of the nested formation algorithm was dedicated to $l3$, the second loop to $l2$, and the last loop to $l1$. The detailed information of thermal units, lines, load power factor, and load distribution rate can be obtained from PowerFactory's library. The ramp rates of thermal units were assumed to be 5 MW/min. The maximum transmission capacity of each line was increased by 25% compared to the base values. Parameter β was assumed to be 60%. The lower and upper voltage limits at each bus in normal operation mode were set to 0.95 p.u. and 1.05 p.u., respectively. The peak demand of the test system was considered to be 290 MW. Also, the critical demands were considered to be 15% of the total demand at each bus. The maximum capacity of WFs placed at buses (partition) 1($l1$), 13($l3$), 14($l3$), and 16($l2$) were equal to 25, 30, 5, 15 MW, respectively. The rated capacity of PV parks located on buses (partition) 7($l1$), 22($l2$), and 27($l3$) were also set to 4, 4, and 6 MW, respectively. To evaluate the effects of tri-state CAES systems on the proposed strategy, four tri-state CAES systems with the capacity of 60 MWh were added to buses (partition) 15($l3$), 16($l2$), 24($l3$), and 28($l1$). The dynamic characteristics of tri-state CAES systems were borrowed from [24]. The operational and maintenance costs of tri-state CAES systems were assumed to be 3.25 $/MW. Also, the natural gas wholesale price was set as 0.11 $/kg [25]. The penalty factors for load and renewable power curtailment, i.e., $VOLL$ and λ^{re}, were considered to be 200 $/MW and 20 $/MW, respectively [25]. The fault duration time, i.e., τ, and the allowable adjustment time of thermal units after unscheduled islanding mode, i.e., $\Delta\tau$, were set to 10 and 2 min, respectively. The uncertainties of wind power, PV power, and electrical loads were handled using Monte-Carlo simulation (MCS) in real-time operational decisions. To this end, one-hundred scenarios were generated by MCS and then reduced to ten scenarios using the GAMS/SCENRED toolbox. The reduced scenarios are shown in Fig. 4, in which the blue lines denote the expected values of the reduced scenarios. In this figure, the shaded portion shows any changes associated with the reduced scenarios relative to the expected values.

Three cases were studied to corroborate the feasibility and effectiveness of the proposed ALOS as follows:

- *Case 1:* Applying the ALOS to the test system only under normal condition;
- *Case 2:* Applying the ALOS with considering both normal and islanding conditions. In this case study, the resilience-target constraints, i.e.,(7a)–(7i), were ignored in the framework of the ALOS;
- *Case 3:* Similar to *Case 2*, but the resilience-target constraints were embedded in the ALOS (our proposed strategy).

These cases are important because, firstly, the behavior of each partition can be analyzed under normal operation mode, and then the

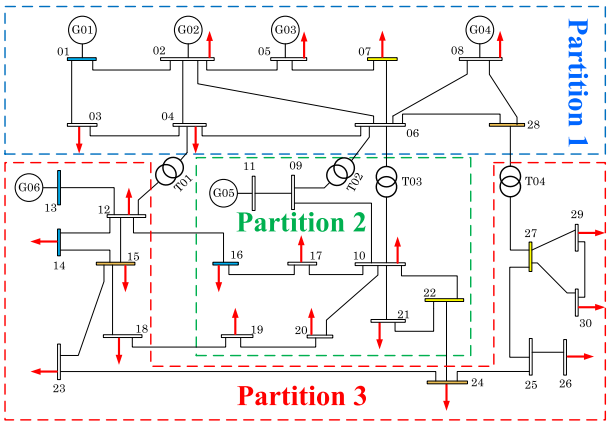

Fig. 3. One-line diagram of the partitioned IEEE 30-bus test system.

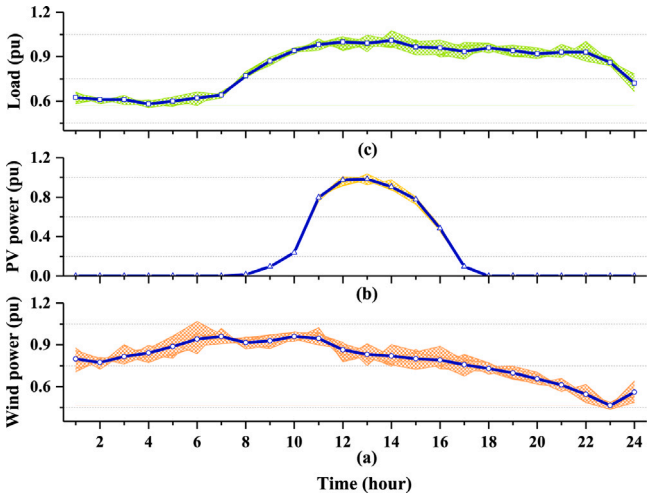

Fig. 4. Scenarios of (a) wind power; (b) PV power; and (c) electrical load.

impacts of the adopted resilient-oriented strategy on maintaining the survival of each partition under stressful condition, i.e., islanding operation, can be investigated. The differences between *cases 2* and *3* would highlight the importance of considering the resiliency constraints.

All case studies were codified as a MILP problem and solved using the CPLEX solver under GAMS environment [26], on a laptop with Intel i7-4500U 1.8 GHz and 6 GB of RAM. The computation times in all studies were less than 240 s, while the mip gap was 0.5%. Computational time is a very important issue in real-time studies. So, to evaluate the computational complexity of the proposed ALOS, the optimization problem was resolved on a computer with AMD Ryzen i9-5000 and 24 GB of RAM using *cloud computing services*. In this case, the computation time was reduced to less than 10 s. It can be concluded that the proposed ALOS is developed with the least level of complexity and can be an ideal option for power system operators to evaluate resiliency-enabling algorithms.

4.2. Results and discussion

To evaluate the performance of the ALOS under the introduced cases, the expected values have been selected as an illustrative scenario, and the simulation results are presented based on them in the next sub-section.

4.2.1. Real-time operation results

Results of implementing ALOS in each partition for each case study are provided in Table 1. As evident from Table 1, in case 1, the proposed strategy was applied to partitions 3, 2, and 1 using the nested formation algorithm, respectively, and all critical and non-critical loads were met using local resources as well as power exchange between adjacent partitions. However, in case 2, when the real-time failures occurred in the common lines between adjacent partitions, the ALOS failed to satisfy the local operational constraints in partition 3. Hence, the optimization results were not feasible in the islanding mode in this partition without considering the resilience-target constraints. As stated in Pseudo-code 1, because the ALOS was infeasible in partition 3, the nested formation algorithm was stopped, and the ALOS was not implemented in partitions 2 and 1. In contrast, once the presented resilience-target constraints were embedded in the ALOS (case 3), the ALOS had reached an acceptable preparedness level to respond to real-time failures and keep all three partitions' normal performance during stressful conditions. Based on Table 1, if the unscheduled islanding mode occurs, the ALOS will be forced to shed 30.566 MWh of non-critical loads in partition 3 to satisfy local operational constraints under case 3. However, other partitions will cover all non-critical loads, i.e., $RI_1 = 1$ and $RI_2 = 1$, in addition to critical loads by relying on their local resources. In other words, the local generation units in partitions 1 and 2 would provide sufficient spinning reserve to cover the critical and non-critical loads located in these partitions when the islanding operation occurs in any period of 24-hour schedule. But, the local generation units in partition 3 have not been able to provide the required spinning reserve to cover the non-critical loads located in this partition to deal with the islanding operation occurring in real-time sessions. Comparison of results in Table 1 clearly indicates that ignoring resilience-target constraints in the ALOS leads to technically infeasible outcomes during islanding mode in the innermost partition.

From an economic point of view, the total operating costs of partitions 3 and 2 were increased from $1,024.941 and $791.5 under case 1 to $7,480.228 and $1,168.717 under case 3, respectively. Therefore, it can be concluded that although the resilience-target constraints guarantee the resilient operation of each partition during unscheduled islanding states, but have led to significant increases in the total operation cost of innermost partitions, i.e., $l3$ and $l2$. It is worth mentioning that the cost of load shedding will be imposed on partition 3 only under the worst-case realization of incidents. Otherwise, this amount, i.e., $6,113.242, will not be part of the daily operating costs of partition 3. On the other hand, comparing case 3 to case 1, it was found that the total operation cost was decreased significantly in the outermost partition, i.e., $l1$.

Based on the presented resilience-target constraints, the ALOS results were revised in case 3 by changing the commitment status of thermal units and tri-state CAES systems compared to case 1. The resulting changes from the thermal units' commitment status in case 3 compared to case 1 are shown in Fig. 5. As one would expect, the total running hour of thermal units in case 3 is more than in case 1. For instance, unit G6 was turned on in case 3 since the beginning of the scheduling period and has had more involvement in the local operation of partition 3 than in case 1, which resulted in a 327.295 USD increment in the operation cost. This happens because by applying the resilience-target constraints, each partition was more risk-averse and prepared more spinning reserve capacity to mitigate the adverse effects of islanding mode as well as to accommodate the uncertainties.

To assess the preparedness level of each partition to handle the islanding mode, in case 3, the prepared spinning reserves in each partition by thermal units and tri-state CAES systems were calculated and compared with the active power exchanged between adjacent partitions in normal mode, as shown in Fig. 6. In this figure, positive amounts indicate the power exports from partition l into the adjacent partitions. The negative amounts correspond to power imports from adjacent partitions into partition l. It can be inferred from Fig. 6

Table 1
Expected operation costs and resiliency index (RI) evaluation report.

Partitions	Case no.	Operation cost of thermal units ($)	Operation cost of CAES systems ($)	Cost of renewable power curtailment ($)	Cost of load shedding ($)	RI_l (%)	Total operation cost ($)
*l*3	Case 1	843.947	178.131	2.863	-	-	1,024.941
	Case 2			INF			
	Case 3	1171.242	192.881	2.863	6,113.242	96.94	7,480.228
*l*2	Case 1	780	0	11.5	-	-	791.5
	Case 2			NS			
	Case 3	880.783	77.5	210.434	0	100	1,168.717
*l*1	Case 1	9,461.987	124.198	0	-	-	9,586.185
	Case 2			NS			
	Case 3	9,252.68	3.25	10.094	0	100	9,266.024

Note: INF-ALOS was infeasible; NS-ALOS was not solved

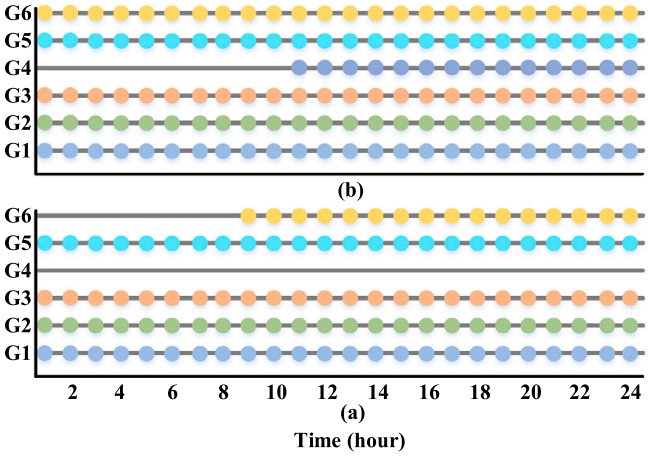

Fig. 5. Thermal units schedule in (a) case 1; and (b) case 3.

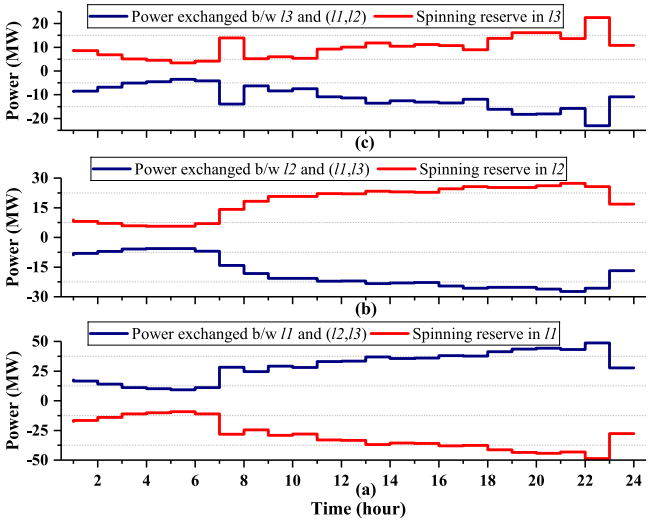

Fig. 6. Comparing total spinning reserve in (a) $l1$; (b) $l2$; and (c) $l3$ with exchanged power between (a) $l1 \leftrightarrow (l2, l3)$; (b) $l2 \leftrightarrow (l1, l3)$; and (c) $l3 \leftrightarrow (l1, l2)$.

that the deployed reserves in partitions 1 and 2 were sufficient and deliverable to cover all critical and non-critical loads locally during the unscheduled islanding mode, which was also expressed in Table 1. However, the spinning reserve provided in partition 3 was 30.566 MWh less than the exchanged power with adjacent partitions during the scheduling period, which will cause to shed non-critical loads during islanding mode.

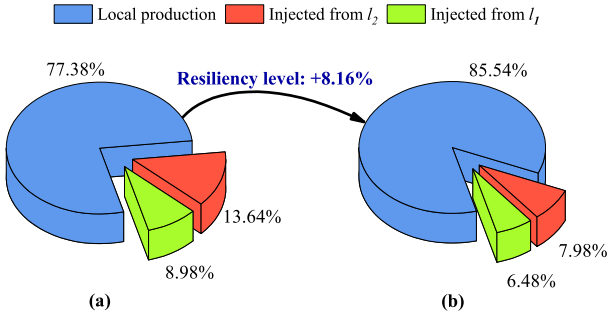

Fig. 7. Optimal mix of sources to meet demands of $l3$ in (a) case 1 and (b) case 3.

For more detailed analysis, Fig. 7 shows the sources used to meet the total demands of partition 3 in cases 1 and 3. As observed, when the ALOS was applied to partition 3 in line with the resilience-target constraints (case 3), the share of local resources, i.e., unit G6, CAES 1, and CAES 3, in the supplying of demands is increased by about 8%. However, this amount is not enough to fully cover the demands of partition 3 under islanding operation mode.

4.2.2. Sensitivity analysis

At first, a sensitivity analysis on the curtailment rate of RESs and RI_l was performed for different amounts of the maximum participation capacity of tri-state CAES systems in expanding, i.e., MC^{exp}, and compressing, i.e., MC^{co}, modes with considering resilience-target constraints (*case 3*) in Table 2. This analysis would help to address one of the main challenges of this study in relation to the opportunities created by multi-carrier energy conversion facilities for real-time emergency control of power systems. To do this, MC^{exp} and MC^{co} were increased/decreased by 10 MW compared to the base values, which in the previous analysis were 20 MW. From Table 2, it can be seen that the curtailment rate of RESs in all partitions is decreased by increasing the values of MC^{exp} and MC^{co}. In addition, with increasing the amounts of MC^{exp} and MC^{co}, RI_3 is increased by up to 99.75% compared to the base case, which will reduce the cost of load shedding in the islanding mode. Therefore, increasing the reservoir capacity of CAES systems can enhance the survivability of the innermost partitions. However, it may result in an increment in the total operation cost of CAES systems. Hence the system operators must consider the optimal trade-off between economic issues and resiliency level.

In next step, the effect of parameter β on the implementation of the ALOS in each partition was analyzed, the results of which are presented in Table 3. To execute this sensitivity analysis, β was increased from 0.5 to 0.7 applying four equal steps. According to the obtained results and efficient frontiers, with increasing the value of β, the curtailment rate of RESs was decreased dramatically in innermost partitions as well as RI_3 was increased from 96.05% to 97.1%. However, when β was set to 0.7,

Table 2
Sensitivity of the ALOS to MC^{exp} and MC^{co} in case 3.

Partitions		$MC^{exp} - MC^{co}$ (MW)		
		10	20 (Base values)	30
$l3$	RI_3 (%)	93.81	96.94	99.75
	Curtailment rate of RESs (MWh)	0.143	0.143	0
$l2$	RI_2 (%)	100	100	100
	Curtailment rate of RESs (MWh)	20.123	10.521	9.31
$l1$	RI_1 (%)	100	100	100
	Curtailment rate of RESs (MWh)	0.504	0.504	0

Table 3
Sensitivity of the ALOS to β in case 3.

Partitions		β				
		0.5	0.55	0.6	0.65	0.7
$l3$	RI (%)	96.05	96.66	96.94	97.03	97.1
	Curtailment rate of RESs (MWh)	5.05	0.143	0.143	0.143	0
$l2$	RI (%)	100	100	100	100	INF
	Curtailment rate of RESs (MWh)	24.79	16.55	10.521	7.687	
$l1$	RI (%)	100	100	100	100	NS
	Curtailment rate of RESs (MWh)	0.504	0.504	0.504	0.504	

Note: INF-ALOS in $l2$ was infeasible; NS-ALOS in $l1$ was not solved.

the ALOS was infeasible in partition 2 during normal operation. In this case, increasing the dependence of the adjunct partitions to each other, i.e. increasing β, can lead to increased internal network congestions on outermost partitions. This means that although increasing β can have positive effects on the innermost partition, it may cause the grid codes to be violated on outermost partitions in normal operation mode. Therefore, it can be concluded that the feasibility of the adopted decentralized scheme and the survivability level of innermost partitions is negatively correlated. Thus, the proposed ALOS can make more conservative decisions to moderate this adverse effect in line with the resilience requirements.

Furthermore, to investigate the impact of the duration time of the islanding operation, i.e., τ, on the total amount of load shedding, sensitivity analysis was performed. For comparison, τ was set from 10 min to 135 min in case 3. The total load shedding of all partitions under different values of τ is shown in Fig. 8. As it is obvious, if the partitioned-based test system operates in islanding mode for $\tau = 75$ minutes (fault clearing time), the total amount of load shedding is equal to 30.566 MWh. According to the obtained results in the previous sub-section, it is clear that this amount is related to partition 3. If the fault clearing time is longer than 80 min, the total amount of load shedding increases linearly. Based on Fig. 8, the islanding operation is feasible only up to $\tau = 135$ minutes, after which the optimization problem will be infeasible. In other words, local resources are only able to supply loads located on each partition for up to 135 min, after which the technical and operational constraints are violated.

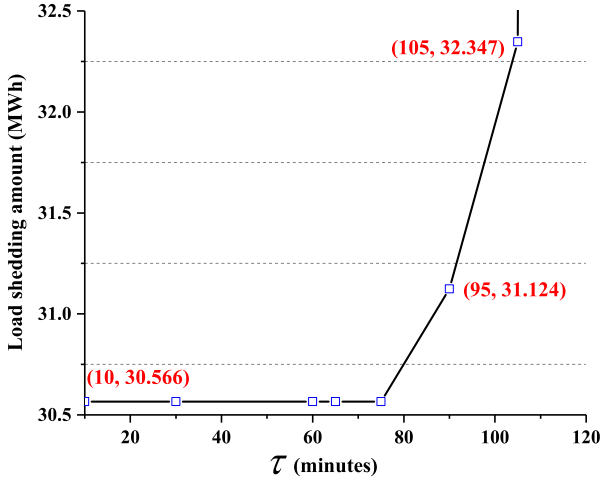

Fig. 8. Sensitivity of total amount of load shedding to τ in case 3.

Table 4
Resiliency index (RI) evaluation under the worst possible series of events in case 3.

	RI (%) in:	
	Only islanding mode	G04 outage condition at the same time as islanding mode
$l3$	96.94	96.94
$l2$	100	100
$l1$	100	100

4.2.3. Accuracy and feasibility of the proposed ALOS

In this sub-section, the contingency analysis was performed by means of DIgSILENT PowerFactory [27] to demonstrate that each partition can survive when exposed to severe disorders under the proposed ALOS. To this end, at first, the impact of different elements on increasing line loading rate was evaluated by considering multiple fault scenarios based on the *n-2* contingencies. The outcomes of the contingency analysis showed that if thermal unit G04, which is connected to bus 8, is out of service, the maximum loading rate will be imposed on transmission lines. Hence, to simulate the worst possible series of events, it is assumed that the unscheduled outage of G04 occurs during the scheduling horizon along with the islanding conditions. Table 4 demonstrates the RI_l in case 3 when the defined disturbances occurred during the real-time session. According to the simulation result, it can be seen that the resiliency index for each partition does not change even in the case of G04 outage during the islanding operation. Therefore, if the defined disturbances occur in real-time, partitions 1 and 2 will be able to handle all local demands without violating the operational constraints. In contrast, 3.06% of non-critical loads on partition 3 will not be met due to the power flow limits. This means that using the proposed strategy, taking advantage of the technical opportunities created by the resiliency constraints, makes it feasible for partitioned-based power system operators to deal with an even larger number of stressful scenarios.

5. Conclusions and future work

This paper took the first steps for the decentralized resilient operation of partitioned-based power systems in the presence of renewable energy sources (RESs) by developing the real-time adaptive local operation strategy (ALOS). The overarching purpose of the proposed ALOS was to operate each partition locally in order from the innermost to the outermost partitions to optimize the local generation resources, i.e., thermal units and tri-state compressed air energy storage (CAES) systems. In addition, the proposed ALOS was sought to take preventive measures for each partition to mitigate the power mismatch in the unscheduled islanding situation, which may be occurring after real-time failures in the common lines between adjacent partitions. The framework was modeled as a two-stage stochastic problem to handle the uncertainties arising from demands and RESs and was solved using the nested formation algorithm. The feasibility of the proposed approach was validated by numerical experiments on the IEEE 30-bus test system. The main conclusions could be drawn as:

- The joint exploitation of the proposed ALOS and set of resilience-target constraints enhanced the preparedness of each partition by increasing the spinning reserve obtained from local resources to survive critical loads and maximize the supply rate of non-critical loads as soon as the islanding mode appears in real-time decisions.
- Compared to traditional resilience-oriented operations, the proposed ALOS was capable to derive appropriate local solutions separately for each partition, which could increase computational accuracy and preserve privacy-preserving requirements in partitioned-based power systems.
- Numerical results showed that the proposed ALOS in coordination with resiliency constraints would supply almost 100% of total critical and non-critical demands during islanding mode, while capturing different sources of uncertainty.
- The use of tri-state CAES systems, in addition to reducing the renewable power curtailment by up to 55%, also played an undeniable role in enhancing the resiliency of each partition.
- The outcomes of this study can help partitioned-based power system operators to understand the local operation of each partition and adopt efficient defense plans for each partition.

The scope of the presented strategy did not include the transient stability analysis during the islanding operation. Hence, the authors' future research endeavor will concentrate on deriving a small-signal model to analyze the stability of each partition as well as the overall system once an unexpected event happens at common lines between adjacent partitions.

CRediT authorship contribution statement

Morteza Zare Oskouei: Conceptualization, Methodology, Software, Writing – original draft. **Hasan Mehrjerdi:** Supervision, Methodology, Project administration. **Davood Babazadeh:** Supervision, Investigation. **Payam Teimourzadeh Baboli:** Writing – review & editing. **Christian Becker:** Formal analysis, Validation. **Peter Palensky:** Formal analysis, Data curation.

Declaration of competing interest

The authors declare that they have no known competing financial interests or personal relationships that could have appeared to influence the work reported in this paper.

References

[1] Zhang R, Hredzak B. Distributed dynamic clustering algorithm for formation of heterogeneous virtual power plants based on power requirements. IEEE Trans Smart Grid 2021;12(1):192–204.

[2] Yin L, Sun Z. Multi-layer distributed multi-objective consensus algorithm for multi-objective economic dispatch of large-scale multi-area interconnected power systems. Appl Energy 2021;300:117391.

[3] Cabiati M, Tornelli C, Martini L. The ELECTRA web-of-cells control architecture concept for the future power system operation. In: 2018 AEIT international annual conference. 2018, p. 1–6.

[4] Oskouei MZ, Mohammadi-Ivatloo B, Erdinç O, Erdinç FG. Optimal allocation of renewable sources and energy storage systems in partitioned power networks to create supply-sufficient areas. IEEE Trans Sustain Energy 2021;12(2):999–1008.

[5] Mishra S, Anderson K, Miller B, Boyer K, Warren A. Microgrid resilience: A holistic approach for assessing threats, identifying vulnerabilities, and designing corresponding mitigation strategies. Appl Energy 2020;264:114726.

[6] European network of transmission system operators for electricity(ENTSO-e). 2021, [Online]. Available:https://www.entsoe.eu/news/2021/01/08/system-split-registered-in-the-synchronous-area-of-continental-europe-incident-now-resolved/.

[7] Ranjbar H, Hosseini SH, Zareipour H. Resiliency-oriented planning of transmission systems and distributed energy resources. IEEE Trans Power Syst 2021;1.

[8] Mehrjerdi H, Saad M, Lefebvre S. Efficiency-resilience nexus in building energy management under disruptions and events. IEEE Syst J 2020;1–10.

[9] Wang X, Li Z, Shahidehpour M, Jiang C. Robust line hardening strategies for improving the resilience of distribution systems with variable renewable resources. IEEE Trans Sustain Energy 2019;10(1):386–95.

[10] Sayed AR, Wang C, Bi T. Resilient operational strategies for power systems considering the interactions with natural gas systems. Appl Energy 2019;241:548–66.

[11] Heckel J-P, Becker C. Dynamic simulation of an integrated energy system for Northern Germany with improved resilience. In: International ETG-congress 2019; ETG symposium. 2019, p. 1–6.

[12] Sedzro KSA, Lamadrid AJ, Zuluaga LF. Allocation of resources using a microgrid formation approach for resilient electric grids. IEEE Trans Power Syst 2018;33(3):2633–43.

[13] Gong L, Fu Y, Shahidehpour M, Li Z. A parallel solution for the resilient operation of power systems in geomagnetic storms. IEEE Trans Smart Grid 2020;11(4):3483–95.

[14] Liu G, Ollis TB, Zhang Y, Jiang T, Tomsovic K. Robust microgrid scheduling with resiliency considerations. IEEE Access 2020;8:153169–82.

[15] Yang C, Yao W, Wang Y, Ai X. Resilient event-triggered load frequency control for multi-area power system with wind power integrated considering packet losses. IEEE Access 2021;9:78784–98.

[16] Cheng Z, Hu S, Yue D, Dou C, Shen S. Resilient distributed coordination control of multiarea power systems under hybrid attacks. IEEE Trans Syst Man Cybern: Syst 2021;1–12.

[17] Ten C-W, Yamashita K, Yang Z, Vasilakos AV, Ginter A. Impact assessment of hypothesized cyberattacks on interconnected bulk power systems. IEEE Trans Smart Grid 2018;9(5):4405–25.

[18] Gan LK, Hussain A, Howey DA, Kim H-M. Limitations in energy management systems: A case study for resilient interconnected microgrids. IEEE Trans Smart Grid 2019;10(5):5675–85.

[19] Ambia MN, Meng K, Xiao W, Dong ZY. Nested formation approach for networked microgrid self-healing in islanded mode. IEEE Trans Power Deliv 2021;36(1):452–64.

[20] Hussain A, Bui V-H, Kim H-M. A resilient and privacy-preserving energy management strategy for networked microgrids. IEEE Trans Smart Grid 2018;9(3):2127–39.

[21] Oskouei MZ, Mohammadi-Ivatloo B, Abapour M, Shafiee M, Anvari-Moghaddam A. Privacy-preserving mechanism for collaborative operation of high-renewable power systems and industrial energy hubs. Appl Energy 2021;283:116338.

[22] Rezvanfar R, Tarafdar Hagh M, Zare K. Power-based distribution locational marginal pricing under high-penetration of distributed energy resources. Int J Electr Power Energy Syst 2020;123:106303.

[23] Akbari T. Approximated MILP model for AC transmission expansion planning: global solutions versus local solutions. IET Gener Transm Distrib 2016;10:1563–9, (6).

[24] Zare Oskouei M, Mohammadi-ivatloo B, Abapour M, Shafiee M, Anvari-Moghaddam A. Strategic operation of a virtual energy hub with the provision of advanced ancillary services in industrial parks. IEEE Trans Sustain Energy 2021;1.

[25] Yan M, Zhang N, Ai X, Shahidehpour M, Kang C, Wen J. Robust two-stage regional-district scheduling of multi-carrier energy systems with a large penetration of wind power. IEEE Trans Sustain Energy 2019;10(3):1227–39.

[26] GAMS solvers. 2017, [Online]. Available at: https://www.gams.com/latest/docs/solvers/index.html.

[27] Zare Oskouei M, Mohammadi-Ivatloo B. Integration of renewable energy sources into the power grid through PowerFactory. 1st ed.. Springer International Publishing; 2020.